Title
Opposing Pressures of Speed and Efficiency Guide the Evolution of Molecular Machines.

Journal
Molecular biology and evolution, 36(12)

ISSN
0737-4038

Authors
Wagoner, Jason A
Dill, Ken A

Publication Date
2019-12-01

DOI
10.1093/molbev/msz190

Peer reviewed

Opposing Pressures of Speed and Efficiency Guide the Evolution of Molecular Machines

Jason A. Wagoner[1] and Ken A. Dill*[,1,2,3]

[1]Laufer Center for Physical and Quantitative Biology, Stony Brook University, Stony Brook, NY

[2]Department of Chemistry, Stony Brook University, Stony Brook, NY

[3]Department of Physics and Astronomy, Stony Brook University, Stony Brook, NY

***Corresponding author:** E-mail: dill@laufercenter.org.

Associate editor: Banu Ozkan

Abstract

Many biomolecular machines need to be both fast and efficient. How has evolution optimized these machines along the tradeoff between speed and efficiency? We explore this question using optimizable dynamical models along coordinates that are plausible evolutionary degrees of freedom. Data on 11 motors and ion pumps are consistent with the hypothesis that evolution seeks an optimal balance of speed and efficiency, where any further small increase in one of these quantities would come at great expense to the other. For F_oF_1-ATPases in different species, we also find apparent optimization of the number of subunits in the c-ring, which determines the number of protons pumped per ATP synthesized. Interestingly, these ATPases appear to more optimized for efficiency than for speed, which can be rationalized through their key role as energy transducers in biology. The present modeling shows how the dynamical performance properties of biomolecular motors and pumps may have evolved to suit their corresponding biological actions.

Key words: **molecular evolution, biomolecular machines, F_oF_1-ATPase.**

Introduction

Biomachines carry out cargo transport, muscle contraction, ATP synthesis, and other jobs in biology. Different jobs require different balances between speed and efficiency. Machines like F_oF_1-ATPase, which synthesizes an organism's ATP, and like myosin II, the motor responsible for muscle contraction, use a large fraction of a cell's energy. So, we expect a large evolutionary pressure on their efficiencies. But speed matters, too, in order to rapidly recharge ATP stores and to generate fast muscle contractions in these examples.

Many biomolecular machines have mechanisms that enable a high speed even at high efficiency: as examples, maintaining a constant torque generation over the angular coordinate of a rotary motor (Oster and Wang 2000), breaking a single large work step into multiple smaller substeps (Anandakrishnan et al. 2016; Wagoner and Dill 2019), the optimization of a machine's conformational free energy landscape (Wagoner and Dill 2019), a transition state location close to the initial state of a machine's mechanical step (Schmiedl and Seifert 2008; Howard 2011; Wagoner and Dill 2016), and the optimal distribution of free energy drops and barrier heights across a cyclic landscape (Brown and Sivak 2017, 2018).

In terms of speed and efficiency, such mechanisms are "win-win": they increase speed without sacrificing efficiency, or vice versa. But, other properties of the machine face a *tradeoff*, where a faster speed comes at the price of lower efficiency (Shoval et al. 2012). As a result, these machines face tough evolutionary choices. For example, myosin II operates at ~35% efficiency during muscle contraction when it hydrolyzes ATP to exert a 6 pN force while taking a 6 nm step (Capitanio et al. 2006; Piazzesi et al. 2007). If myosin II were to instead exert a higher force, muscle contraction would have a higher efficiency but slower speed. As another example, the F_oF_1-ATPase of animal mitochondria operates at 80–90% efficiency as it pumps eight protons downhill to synthesize three ATP molecules (Watt et al. 2010). As we show below, if it were instead to pump nine protons, it could recharge depleted ATP stores faster, but less efficiently.

Here, we use modeling to study these evolutionary tradeoffs: not just *what is*, but *what could have been*. We include plausible evolutionary control parameters–such as the force exerted by myosin II or the number of protons pumped by F_oF_1-ATPase–to explore how molecular machines can be optimized. We derive expressions for the optimal work output for simple machines. Comparing in vivo data across a range of machines, we give evidence that evolution tends toward mechanisms that give an optimal balance of speed and efficiency, where any further small increase in one of these quantities would come at great expense to the other. We show how pressures on speed and efficiency have guided the evolution of the c-ring of F_oF_1-ATPase, which determines the number of protons pumped per ATP synthesized by the motor.

Results and Discussion

Calculating the Speed and Efficiency of a Simple Molecular Machine

Figure 1 shows a model of a simple molecular machine. It converts the free energy put into the system, $\Delta\mu \geq 0$, for

Article

example, from ATP hydrolysis, into work performed by the system, $w \geq 0$. The machine has two steps: a nonmechanical transition ($A_j \rightarrow B_j$), which may include chemical and/or conformational changes, and a mechanical transition ($B_j \rightarrow A_{j+1}$), over which the machine performs work. The cycle repeats periodically: the subscript j labels the position along the track or the number of forward cycles completed. Although simple, this model is able to capture essential features of how a machine can best convert its input free energy into output work (Wagoner and Dill 2019).

We model a machine's operation in a nonequilibrium steady state. Here, we call the difference between the input, chemical work $\Delta\mu$ and the output work w the net drop in *basic free energy* across the machine cycle: $\Delta\mu_{\text{net}} = (\Delta\mu - w) \geq 0$. The net basic free energy $\Delta\mu_{\text{net}}$ is a measurable quantity. It resembles an equilibrium free energy, but it is corrected for nonequilibrium effects, such as a difference in concentrations of species that are out of equilibrium (e.g., [ATP]) (Hill 1977; Wagoner and Dill 2019) (Note.—The decrease in basic free energy is referred to elsewhere as the *energy dissipation* or sometimes *free-energy dissipation* that maintains the nonequilibrium steady state. Here, we use the term *basic free energy* exclusively.). We define the thermodynamic efficiency of a machine as:

$$\eta = \frac{w}{\Delta\mu} = 1 - \frac{\Delta\mu_{\text{net}}}{\Delta\mu}. \quad (1)$$

We also use this model to calculate the cycle flux $J = \tau^{-1}$, where τ is the cycle time of the machine (see Materials and Methods). We use "speed" to refer to the flux, velocity, or current of a machine. For a cytoskeletal walker like myosin, the velocity is $V = Jd$ for a step size d. For an ion pump, the current $I = nJ$ for n ions transported per cycle.

An important factor in determining the speed of a machine is how the basic free energy changes are distributed across different transitions (Brown and Sivak 2017; Wagoner and Dill 2019), see Materials and Methods. We define the quantity λ as the fraction of free energy from the input chemical work that is expended across the mechanical step and label two limiting cases. We call a small value of $\lambda \approx 0$ a *ratchet* machine because the basic free energy that is available from input chemical energy is expended in the nonmechanical (first) step and all the work is performed in the mechanical (second) step. We call a large value of $\lambda \approx 1$ a *driven* machine because the available energy is expended across the work (second) step (Wagoner and Dill 2019). Below, we use this classification to describe the evolution of different types of machines.

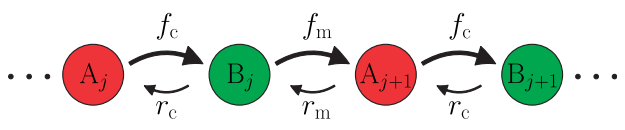

Fig. 1. A two-state machine with one nonmechanical step (c) and one mechanical step (m). The first, nonmechanical step ($A_j \rightarrow B_j$) does not perform work and includes chemical or conformational changes of the machine. The second, mechanical step ($B_j \rightarrow A_{j+1}$) performs work and generates the machine's output (e.g., the mechanical step of myosin along an actin filament).

Capturing the Tradeoffs between Speed and Efficiency in Molecular Machines

Figure 2 shows the in vivo efficiencies for 12 biomolecular machines. The efficiency is >80% for four of the machines shown and >50% for nine of them, meaning these machines are as efficient as macroscopic electric motors and are more efficient than heat engines. We have chosen to study these 12 machines because their values of input free energy $\Delta\mu$ and output work w, used to calculate efficiency, are known and appear to be consistent over cell conditions and different experimental measurements, see supplementary section I, Supplementary Material online.

Although these machines are quite efficient in vivo, there is considerable variation, and the in vivo work w is not well correlated with $\Delta\mu$. We hypothesize that some of these differences may reflect an evolutionary optimization based on the different jobs they perform and based on the tradeoff between speed and efficiency. We want a measure of machine *performance* that can capture these effects. For macroscopic thermal engines and molecular machines, a common measure of performance is the *power output*, the work per unit time τ (Van den Broeck 2005; Schmiedl and Seifert 2008). Since the efficiency is $\eta = w/\Delta\mu$, we can define the power output per unit input energy as follows:

$$F(\theta) = \frac{(\eta(\theta))^{\alpha}}{\tau(\theta)}, \quad (2)$$

where θ indicates some variable of the machine to be optimized, and α is a positive constant $0 < \alpha < \infty$. Optimizing F for an individual machine is equivalent to optimizing the power output of a set of machines working together in some function like muscle contraction, see supplementary section II, Supplementary Material online. Equation (2) has the properties we seek in a performance function: F increases with respect to greater speed and with respect to greater efficiency. And, the constant α recognizes our ignorance about whether speed or efficiency might be more important to biological

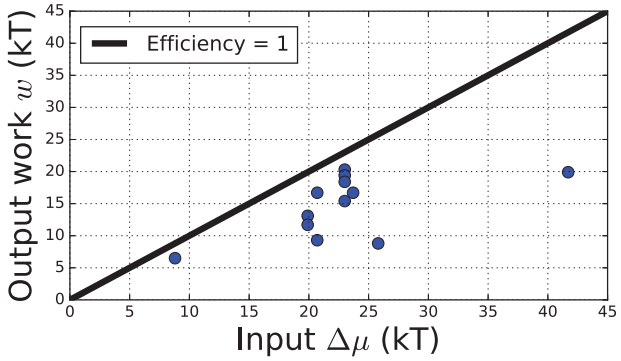

Fig. 2. The in vivo efficiencies of molecular machines. Included are Na-K ATPase; SERCA; the proton PP_i pump; PMCA; V-ATPase; myosin II; NCX; NCKX; and animal, *Escherichia coli*, and chloroplast F_0F_1-ATPase.

evolution. The standard definition of performance as power per unit energy input corresponds to $\alpha = 1$.

We first ask, how much work w should a machine perform in order to have optimal performance? Using the two-state model above, we maximize $F(w)$ with respect to the work w. In the absence of an analytical solution, we determine approximate solutions for the two limiting cases of a ratchet machine "r" (large $\Delta\mu$, small λ, $\delta > 0.2$) and a driven machine "d" (large $\Delta\mu$, large λ), see supplementary section III, Supplementary Material online. The speed-efficiency tradeoffs for these two cases are shown in figure 3*a*. The optimal work output for these cases is:

$$w_{\mathrm{opt}}^{(\mathrm{r})} \approx \frac{\mathrm{kT}}{\alpha\delta}, \tag{3}$$

$$w_{\mathrm{opt}}^{(\mathrm{d})} \approx \lambda\Delta\mu - \mathrm{kT}\ln[\beta\lambda\Delta\mu] + \mathrm{kT}\ln\alpha - \mathrm{kT}\ln\left[1 + e^{-\beta(1-\lambda)\Delta\mu}\right]. \tag{4}$$

These equations show that the optimal work for a ratchet machine is small (a few kT), while the optimal work for a driven machine is large; see figure 3*b*. This is because a ratchet machine has an *unfavorable* tradeoff: as shown in figure 3*a*, it can be fast or efficient, but not both. Increasing the efficiency greatly slows down the machine, and so the optimal work output is small. In contrast, the driven machine has a *favorable* tradeoff: the machine can be both fast and efficient simultaneously and the optimal work output is large.

Are these predictions valuable for real machines? That depends on how much we know about the exact evolutionary pressures on speed versus efficiency. We express these variable pressures with the parameter α in equation (2). Because a ratchet machine can be fast or efficient, but not both, $w_{\mathrm{opt}}^{(\mathrm{r})}$ depends strongly on α, shown by the broad, red contours of figure 3*b*. This does not give a useful prediction for real machines unless we know the exact evolutionary pressures on speed versus efficiency.

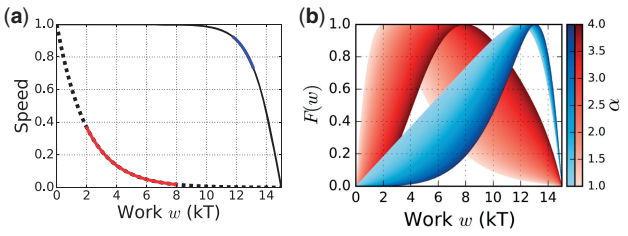

FIG. 3. (*a*) Ratchet machines (dashed line) can be either fast or efficient, but not both. Driven machines (solid line) can be fairly good at both speed and efficiency. Here, $\lambda = 0$ and 1 for the ratchet (dashed) and driven (solid) machines, respectively. The regions highlighted in red and blue correspond to the optimal values of work output over the range $\alpha \in [1, 4]$. For these machines, $\Delta\mu = 15$ kT, $\delta = 0.5$, and $g_{\mathrm{c}}^{\ddagger} = g_{\mathrm{m}}^{\ddagger}$. (*b*) Optimal ratchets perform less work than optimal driven machines. The colors are shaded by the quantity $\alpha \in [1, 4]$, which defines a range of possible performance criteria in equation (2). The narrow blue contours show that w_{opt} for a driven machine is insensitive to varying evolutionary pressures on speed versus efficiency, while the broad red contours show that the ratchet machine is more sensitive to these varying pressures.

The driven machine, on the other hand, can achieve an *optimal balance* of speed and efficiency. At this value of $w_{\mathrm{opt}}^{(\mathrm{d})}$, any further slight increase in speed would come at great expense to efficiency, or vice versa, as shown in the blue tradeoff curve of figure 3*a*. Therefore, $w_{\mathrm{opt}}^{(\mathrm{d})}$ only weakly depends on α, shown by the thin, blue contours of figure 3*b*. Here, $w_{\mathrm{opt}}^{(\mathrm{d})}$ changes by only 11% over the range $\alpha \in [1, 4]$ (maxima of the blue contours in fig. 3*b*) while, for the ratchet machine, $w_{\mathrm{opt}}^{(\mathrm{r})}$ varies by 300% over the same range. We hypothesize that driven machines will evolve toward this value of $w_{\mathrm{opt}}^{(\mathrm{d})}$ since the prediction does not require that we know much about whether speed or efficiency is more important to evolution, as long as the exact pressures are not too extreme.

We next test this prediction for 11 of the machines shown in figure 2. We use the experimentally measured values of standard ($\Delta\mu^0$, w^0) and chemiosmotic ($\Delta\mu'$, w') contributions to input free energy and work and set $\lambda = \Delta\mu^0/\Delta\mu$, see Materials and Methods. We then split these machines into two classes. Class 1 contains the *driven* motors myosin II, NCX, NCKX, Animal F_oF_1-ATPases, and *Escherichia coli* F_oF_1-ATPase. Class II contains the *ratchet* machines. These are ion pumps that work primarily against chemiosmotic gradients: Na-K ATPase, SERCA, the proton PP_i pump, PMCA, and V-ATPase. We now study the speed-efficiency tradeoffs of these machines over different evolutionary degrees of freedom.

Motor Performance Is Controlled by the Demands of Input Free Energy and Output Work

We computed the performance landscape $F(\Delta\mu^0, w^0)$ of a driven motor as a function of degrees of freedom $\Delta\mu^0$ and w^0 by calculations detailed in supplementary section IIID, Supplementary Material online. In addition, we are able to calculate the peak performance ridgeline analytically, from the two leading terms of equation (4):

$$w_{\mathrm{opt}}^{0} \approx \Delta\mu^0 - \mathrm{kT}\ln[\beta\Delta\mu^0]. \tag{5}$$

Our calculated performance landscape is shown in figure 4. The red dots show the experimental data for five class I (driven) biomolecular machines. The fact that the data fall in such a tight cluster along the predicted ridgeline supports the contention that evolution has sought an optimal balance of speed and efficiency. Motors may have undergone structural evolution that systematically changes $\Delta\mu^0$ or w^0 to optimize their performance as given by F. And, the sharpness of the ridgeline indicates how steeply the performance is predicted to fall off with small changes in those degrees of freedom.

What are the properties of motors that evolve to achieve these results? We assume a separation of evolutionary timescales, where some properties of these motors are fixed while others are optimizable degrees of freedom. For F_oF_1-ATPase, we might assume the work w^0 of synthesizing ATP is fixed and the evolutionary degree of freedom is the input $\Delta\mu^0$, which depends on the membrane potential and the number of protons transported by the motor. For myosin II, we might

suppose that the input free energy $\Delta\mu^0$ gained from ATP hydrolysis is fixed. Then, evolution can change $w^0 = fd$ by changing the force f exerted or the step size d. During muscle contraction, myosin II exerts a force $f = 6$ pN against a step of $d = 6$ nm over a wide range of conditions (Piazzesi et al. 2007). This gives $w^0 \approx 9$ kT, which is in good agreement with the predicted $w^0_{\text{opt}} = 9.8$ kT shown in figure 4. Cellular regulatory mechanisms might further fine-tune motors to keep them operating at this peak performance against varying conditions of the cell, see Supplementary section IIIF, Supplementary Material online.

The Performance of Ion Pumps Depends on the Numbers of Ions Transported per Cycle

Now, in a similar fashion, consider the performance function for ion pumps. These proteins pump against chemiosmotic gradients, which indicates that they are ratchet-like, $\lambda \approx 0$ (see Materials and Methods). What evolutionary degrees of freedom should we consider in this case? If we were to again assume that the output work w is a degree of freedom, then equation (3) predicts that the optimal output work should be small (a few kT, depending on model parameters). This is not observed; SERCA, for example, pumps a Ca^{2+} ion against a 20,000-fold concentration gradient, $w \approx 18$ kT (Toyoshima 2009). We conclude that these large concentration gradients are essential to cell function and that output work is not an appropriate degree of freedom in this case.

Instead, we assume that ion pump *stoichiometry* is a relevant evolutionary degree of freedom. For example, a calcium pump could evolve to pump one, two, or more ions per ATP hydrolyzed. In this case, we take the total work to be $w = Mw_{\text{ion}}$, where w_{ion} is the work of pumping a single ion and M is the number of ions pumped per cycle. We again assume a separation of evolutionary timescales, where $\Delta\mu$ (from ATP hydrolysis for all pumps studied here) and w_{ion} (from the large concentration gradients) are important to cell function at their given values and therefore fixed, while M is an evolutionary degree of freedom that can be optimized by an ion pump.

So, for ion pumps, what is the optimal value $M = M_{\text{opt}}$ that maximizes the performance $F(M)$? Figure 5 shows the computed performance F as a function of $\Delta\mu$ and w_{ion}, which are fixed, and of M, which is the evolutionary degree of freedom. And, we are able to calculate the peak performance ridgeline as (see supplementary section IIIE, Supplementary Material online):

$$\frac{\Delta\mu}{M_{\text{opt}}} \approx w_{\text{ion}} + \text{kTln}[\beta w_{\text{ion}}] - \text{kTln}\ \alpha. \qquad (6)$$

Equation (6) is the model's prediction for the evolutionary state toward which ion pumps will evolve. In this case, too, the data from six ion pumps fall closely along the ridgeline, indicating consistency with this evolutionary hypothesis. The predicted values M_{opt} are found to be in exact agreement with the true values of M for these pumps (see supplementary section IIIE, Supplementary Material online), except for Na-K ATPase, which pumps five ions, in contrast to the model prediction of $M_{\text{opt}} = 4$. This predicted value may be off either because the model is too simple or because there is a high evolutionary pressure on efficiency, which would be sensible given that Na-K ATPase consumes a particularly large amount of a cell's total ATP (Paul 1965; Buttgereit and Brand 1995; Howarth et al. 2012).

These pumps have a favorable speed-efficiency tradeoff with respect to the ion stoichiometry M (see supplementary section IIIE, Supplementary Material online), and so once again it appears that they evolve toward this value of M_{opt} because it gives an optimal balance between speed and efficiency. Pumping fewer ions per ATP cycle would sacrifice efficiency at no gain to turnover speed because pumping against a large chemiosmotic gradient (e.g., for SERCA,

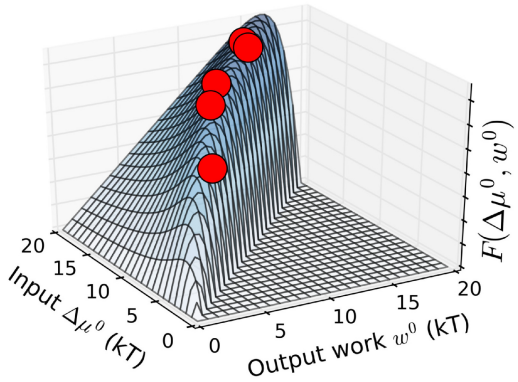

FIG. 4. Driven biomachines appear to be optimized for performance as a function of input free energy and output work. Performance is given by $F(\Delta\mu^0, w^0)$, the power output per energy input, equation (2). The red dots show the in vivo observed values of input free energy $\Delta\mu^0$ and output work w^0 for myosin II, NCX, NCKX, PMCA, Na-K ATPase, Animal, and *Escherichia coli* F_0F_1-ATPase. The locations of the red dots along the peak ridgeline indicate that these motors appear evolutionarily optimized for performance.

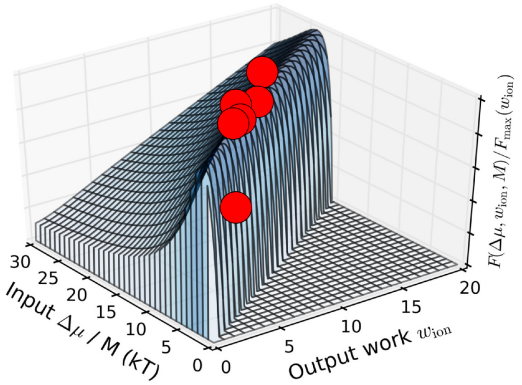

FIG. 5. The performance landscape for ion pumps. We assume that the total input $\Delta\mu$ and work per ion w_{ion} are fixed, while the pump stoichiometry M is an evolutionary degree of freedom. $F(\Delta\mu, w_{\text{ion}}, M)$ is the power output per energy input, equation (2). The landscape is calculated over the input free energy and output work per ion pumped, $\Delta\mu/M$ and w_{ion}. These ion pumps closely match our prediction for optimal stoichiometry from equation (6). The landscape is normalized over the axis of output work because we assume that w_{ion} is not an evolutionary degree of freedom.

binding intracellular Ca^{2+} at nanomolar concentrations) cannot be sped up by dissipating more energy. For both motors and ion pumps, the output power per unit free-energy input resembles an evolutionary fitness because it defines the positions of optimal balance between speed and efficiency.

F_oF_1-ATPase Can Evolve Different Numbers of c-Ring Subunits

Above, we considered what outputs are optimal to meet the environmental and performance requirements of molecular machines. Here, for F_oF_1-ATPase in particular, we give a more granular model of how evolutionary changes can be encoded in the motor's *molecular structure*. F_oF_1-ATPase uses a rotary mechanism to synthesize ATP, see figure 6. F_o, which is the membrane domain, takes as input the downhill transport of 8–15 protons, depending on the species (Pogoryelov et al. 2012). During proton transport, F_o rotates to generate energy that, through the central shaft γ, is transmitted to the F_1 domain. F_1, which is peripheral to the membrane, synthesizes three ATP molecules per full 360° rotation of F_o. The rotary mechanism intersperses the downhill steps of proton transport with the uphill steps of ATP synthesis, which are subdivided into separate work steps of reactant binding, synthesis, and product release (Watanabe et al. 2011; Adachi et al. 2012; Suzuki et al. 2014). The part of F_o that rotates is the c-ring. The c-ring is composed of N identical c-subunits, each of which transports one proton per 360° rotation. Interestingly, the numbers of c-ring subunits vary across different species, ranging from $N = 8$ (animal; Watt et al. 2010) to $N = 15$ (*Spirulina platensis*; Pogoryelov et al. 2009). The value of N is constant within a species (Pogoryelov et al. 2012). The number N of c-ring subunits can be changed by as few as one or two mutations (Pogoryelov et al. 2012; Preiss et al. 2013). This implies that N is a key evolutionary degree of freedom through which F_oF_1-ATPase adapts to different membrane environments across species (von Ballmoos et al. 2009).

The efficiency and the ATP synthesis rate (i.e., the speed) of F_oF_1-ATPase depends on its membrane environment, given by the membrane potential $\Delta\psi$ and the chemiosmotic gradient across the membrane ΔpH. The components $\Delta\psi$ and ΔpH sum together to give the proton motive force (PMF), that is, the free energy gained by transporting one proton across the membrane:

$$\Delta\mu_{H^+} = 2.3\Delta\text{pH} - F_e\Delta\psi, \tag{7}$$

where F_e is Faraday's constant and the gradients $\Delta\psi$, ΔpH are defined relative to outside. The efficiency of the motor can be computed as follows:

$$\eta = \frac{3\Delta\mu_{ATP}}{N\Delta\mu_{H^+}}, \tag{8}$$

where $\Delta\mu_{ATP}$ is the free energy of synthesizing an ATP molecule.

The Performance of F_oF_1-ATPase Depends on Membrane Environment and c-Ring Stoichiometry

To study the evolution of F_oF_1-ATPase across different species, we calculate its efficiency and synthesis rate with respect to different values of the c-ring stoichiometry N and with respect to different membrane environments; see Materials and Methods for a description of these calculations. For many species, the total PMF is about the same, $\Delta\mu_{H^+} \approx 180 - 210$ mV or 7–8 kT per proton that is pumped. But, the relative contributions from ΔpH and $\Delta\psi$ to this PMF vary, with $\Delta\psi = -30$ to -150 mV (see supplementary section IVC, Supplementary Material online).

Figure 7*a* shows the computed ATP synthesis rate of F_oF_1 with respect to two degrees of freedom: $\Delta\psi$ and N. We take the membrane potential $\Delta\psi$, with the total PMF held constant at $\Delta\mu_{H^+} = 200$ mV, to reflect the in vivo environments of different species. So, a $\Delta\psi$ of smaller magnitude signifies a larger ΔpH. This figure shows two trends. First, synthesis rate increases for larger magnitudes of $\Delta\psi$, then decreases. A

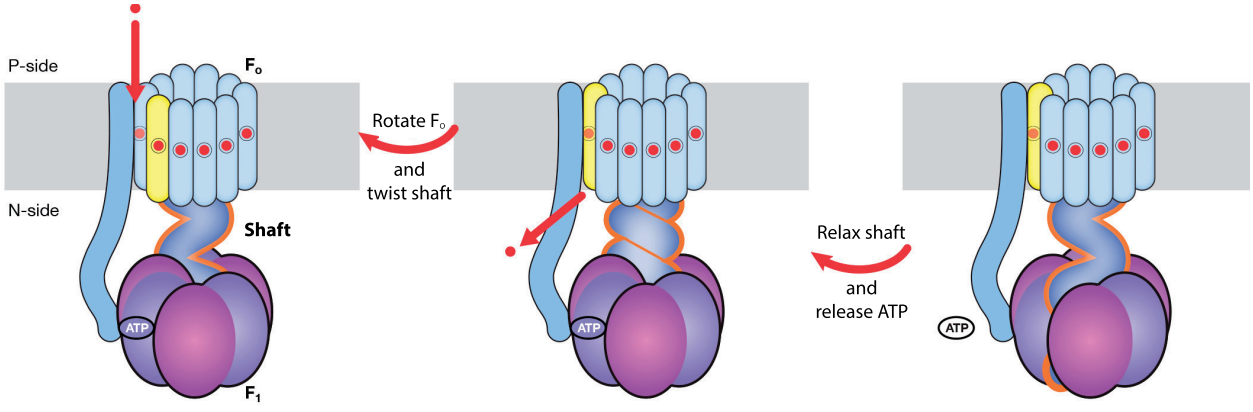

FIG. 6. The structure and function of F_oF_1-ATPase. The F_o domain is integral to the membrane and contains the c-ring, which rotates as it transports protons downhill across the membrane. The energy gained from this rotation is transmitted through the intermediate elastic linker (the γ subunit) to F_1, the peripheral membrane domain. F_1 synthesizes three ATP molecules for each full 360° rotation of F_o. This illustrates one portion of the total cycle. Across the first transition (left to center panels), F_o transports one proton and the c-ring rotates. This increases the elastic strain on the central shaft. Across the second transition (middle to right panels), this tension is relieved as F_1 undergoes a conformational change and releases newly synthesized ATP.

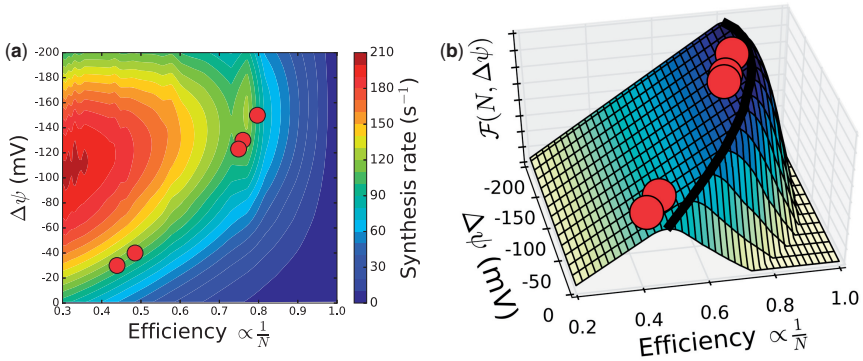

Fig. 7. (*a*) The speed and efficiency of F_oF_1-ATPase with respect to different membrane environments and with respect to the c-ring stoichiometry *N*. The efficiency is inversely proportional to *N*, see equation (8). Plotted in red are the experimentally determined in vivo efficiencies (corresponding to different values of *N* from 8 to 15) and membrane environments of F_oF_1 for five species, from left to right: *Spirulina platensis*, spinach chloroplast, *Saccharomyces cerevisiae*, *Escherichia coli*, and animal mitochondria. (*b*) The performance landscape of F_oF_1-ATPase with respect to different membrane environments and with respect to the c-ring stoichiometry *N*. The efficiency is inversely proportional to *N*, see equation (8). On the *z* axis is the *performance function* of equation (9), with the peak ridgeline shown in black for the threshold $J_c = 65\ s^{-1}$. Plotted in red are the experimentally determined in vivo efficiencies and the membrane environments for the same five species. For both plots, the total PMF is $\Delta\mu_{H^+} = -200$ mV, but with different contributions from $\Delta\psi$ and Δ pH, and $\Delta\mu_{ATP} = 18.0$ kT.

larger $\Delta\psi$ gives a bigger free energy drop across the mechanical step as F_o rotates and increases the elastic strain on the central shaft (see Materials and Methods). This agrees with our previous work, which showed that the fastest machines are those having an optimal value of the free energy drop across the mechanical step, because this overcomes the kinetic barriers of performing uphill work (Wagoner and Dill 2019). The second trend is that motors are faster if the c-ring has more subunits (larger *N*). Larger *N* increases the motor's gear ratio. That is, greater synthesis rates can be achieved by partitioning the total work of ATP synthesis into smaller substeps (Anandakrishnan et al. 2016; Wagoner and Dill 2019).

Figure 7*a* also shows the experimentally determined *N* values and in vivo membrane environments for five different species. How should we interpret the positions of these data points? First, we note that the data fall into a narrow (blue-green) region of the plot, indicating evolution toward a specific synthesis rate, regardless of species. But based on what principle? What property might these machines be optimizing? Following equation (2), we hypothesize again the importance of *power output*, a product of efficiency with speed,

$$\mathcal{F}(N,\Delta\psi) = \begin{cases} \eta(N,\Delta\psi)J(N,\Delta\psi) & J < J_c \\ \eta(N,\Delta\psi)J_c & J \geq J_c \end{cases}, \quad (9)$$

where *J* is the synthesis rate and J_c is a threshold constant. This function $\mathcal{F}$ optimizes efficiency alone, as long as the synthesis rate is above some threshold J_c, and punishes synthesis rates that are below this threshold. Here, $J_c = 65 \pm 35\ s^{-1}$ (for sensitivity analysis, see Materials and Methods and supplementary section IVB, Supplementary Material online). So, this performance function reflects a greater importance of efficiency. This makes sense since so much of an organism's ATP content is synthesized by this motor.

Figure 7*b* shows the landscape of this performance function $\mathcal{F}$. The data fall along the peak ridgeline. We draw the following conclusions. First, at high efficiencies, the highest synthesis rates are given when $\Delta\psi \approx -150$ mV (fig. 7*a*). This is the value of the membrane potential of animal mitochondria. As a result, animal F_oF_1 sits near the global optimum of the performance landscape in figure 7*b*. This suggests that, in addition to c-ring stoichiometry *N*, the membrane potential $\Delta\psi$ may be an evolutionary degree of freedom that has been optimized in some species. The data support this hypothesis for animal mitochondria, as well as for *E. coli* and *Saccharomyces cerevisiae*.

For chloroplast and *Spirulina platensis*, however, this does not appear to be the case. Both of these species have a low membrane potential. A larger magnitude $\Delta\psi$ in chloroplasts or *Spirulina platensis* appears to cause photoinhibition (Checchetto et al. 2012) and so may not be an evolutionary option. Therefore, it appears that these species have evolved their c-ring stoichiometries for high efficiencies, while avoiding synthesis rates that are too low. Figure 7*a* indicates that a greater efficiency (a smaller c-ring) for chloroplasts or *Spirulina platensis* would result in synthesis rates that may be unacceptably low.

A Broader Context and Implications for Design and Disease

Our work indicates what degrees of freedom–and what constraints–might be active in evolution to optimize a machine's thermodynamic performance. Here, the free-energy obtainable from ATP hydrolysis has been taken to be fixed, while the c-ring stoichiometry of F_oF_1-ATPase is known to be alterable by as few as one or two mutations (Pogoryelov et al. 2012; Preiss et al. 2013). Similarly, myosin's step size can change through point mutations to the light chain (Sherwood et al. 2004) or by changing number of IQ motifs that compose the tail domain (Sakamoto et al. 2005).

Where there are degrees of freedom, a few mutations can also, in principle, lead to disease states. Figures 4, 5, and 7*b* show that a small change in a machine's degree of freedom can lead to a steep dropoff in its performance. Disregarding

loss-of-function mutations, there are indeed diseases that result from mutations that diminish the performances of these machines. Examples include Na-K ATPase (familial hemiplegic migraine) (Spiller and Friedrich 2014; Clausen et al. 2017), F_oF_1-ATPase (neurodegenerative syndromes) (Kucharczyk et al. 2009; Dautant et al. 2018), SERCA (Darier Disease and potentially Parkinson's disease) (Ahn et al. 2003; Lee et al. 2019), NCX (cardiac fibrillation) (Langenbacher et al. 2005), and myosin (cardiomyopathy, hearing loss) (Greenberg et al. 2010; Lin et al. 2011).

Finally, we note that the present model fits into a broader context. Recently, other studies have given insight into properties of evolution by studying the thermodynamics of proteins and cell machinery (Sikosek and Chan 2014; Kalapis et al. 2015). For example, the cellular machinery of *proteostasis*, the cell's network of biomolecules that fold and disaggregate and chaperone the proteome to ensure its folding health, has evolved to achieve a balance of energy and chaperone abundances needed to make effective trafficking decisions (Santra et al. 2017; Agozzino and Dill 2018). Further, this machinery and a protein's stability can affect genetic variation and the speed of evolution (Sabater-Muñoz et al. 2015; Agozzino and Dill 2018). Protein stability also has tradeoffs with new protein functions (Tokuriki et al. 2008; Sikosek et al. 2012) and with enhanced enzymatic activities (Klesmith et al. 2017). Future work that identifies the molecular mechanisms underlying these different tradeoffs may give new therapeutic strategies for the aforementioned diseases and may give a route for directed evolution to optimize molecular machines for biotechnology applications.

Conclusions

We have explored evolutionary tradeoffs of speed and efficiency in biomolecular motors and ion pumps. Although some machines, such as kinesin (not studied here), have broad ranges of operating conditions of loads or forces, the machines studied here all operate over relatively narrow ranges of input free energy and output work in vivo. Using simple dynamical models and plausible choices of evolutionary degrees of freedom–such as the force exerted by myosin II, the number of ions transported by an ion pump, and the c-ring stoichiometry of F_oF_1-ATPase–we find that these machines achieve an optimal balance of speed and efficiency. In many cases, the property that appears to be optimized, serving the role of evolutionary fitness, is the *power out per unit energy in*.

Materials and Methods

Calculating the Speed of the Two-State Molecular Machine

Figure 1 shows the two-state molecular machine. We can calculate the cycle flux J (number of full cycles per unit time) of this machine as (Wagoner and Dill 2019):

$$J = \frac{f_c f_m - r_c r_m}{f_c + f_m + r_c + r_m} = \tau^{-1}, \tag{10}$$

where the rate constants are shown in figure 1. We use rate definitions that we have shown can accurately reproduce experimentally measured dynamics for a range of molecular machines (Wagoner and Dill 2019):

$$\begin{aligned} f_c &= k_0 e^{-\beta(g_c^\ddagger - (1-\lambda)\Delta\mu)} r_c = k_0 e^{-\beta g_c^\ddagger} \\ f_m &= k_0 e^{-\beta(g_m^\ddagger - \lambda\Delta\mu + w\delta)} r_m = k_0 e^{-\beta(g_m^\ddagger - w(1-\delta))} \end{aligned} \tag{11}$$

where k_0 is a frequency factor, and $g_c^\ddagger$, $g_m^\ddagger$ are intrinsic barriers common to both the forward and reverse transitions.

The dimensionless parameters δ and λ are descriptors of the shape of the machine's landscape. The parameter δ represents the location of the transition state along the mechanical step, which dictates how a change in w effects the forward and reverse barrier heights of the mechanical step (Howard 2011; Wagoner and Dill 2016). The parameter λ gives the fraction of free energy from the input chemical work that is expended within the mechanical step (Wagoner and Dill 2019). λ describes an inherent feature of the machine–how free energy changes are distributed across the machine's cyclic landscape, independent of the amount of work w it performs. The value of λ implicitly includes two contributions, from the input chemical energy $\Delta\mu$ and from changes in conformational free energy, which must sum to zero across the full cycle.

As described in the main text, we define two limiting cases of a *ratchet* machine (a small value $\lambda \approx 0$) and a *driven* machine (a large value $\lambda \approx 1$). In some literature, our term *ratchet* is what others call a Brownian or Feynmann ratchet, and our term *driven machine* is what others call a power stroke motor (Astumian et al. 2016). We do not use these terms here in order to avoid confusion with their other multiple definitions in the field. We define *ratchet* and *driven* machines narrowly, in terms of small and large value of λ, respectively.

Modeling the Evolutionary Changes in Speed and Efficiency of Biomolecular Machines

In order to study the optimization of biological machines over different evolutionary degrees of freedom, we first define a simple model for their dynamics. For the 12 machines listed in figure 2, the in vivo values of input free energy $\Delta\mu$ and output work w are known. However, other details–such as the distribution of basic free energy changes expressed through λ in equations (11), and how λ would change over different evolutionary degrees of freedom–are generally not known. To find a simple model to estimate λ, we note that the available free energy can be written as $\Delta\mu = \Delta\mu^0 + \mathrm{kTln}c_2/c_1$, where the first term is a standard contribution and the second is a chemiosmotic term due to concentration differences. We assume that only the first term $\Delta\mu^0$ is extractable here in the mechanical step, and thus we set $\lambda = \Delta\mu^0/\Delta\mu$ and use the two-state model to calculate machine speeds. To calculate the landscape in figure 4, it is important to also separate the output work into standard w^0 and chemiosmotic w' contributions, see supplementary section IIID, Supplementary Material online.

In short, for a machine driven by an ionic gradient, this model assumes that the free energy gained from pumping one charge downhill ($\Delta\mu^0$) can be used to lower the electrostatic barrier of pumping another charge uphill (w^0). For a machine driven by ATP hydrolysis, this model sets the free

energy drop across the mechanical step to the intrinsic free energy available in the chemical bond, $\Delta\mu^0_{ATP}$, independent of concentration differences. This matches the intuition of early models that $\Delta\mu^0_{ATP}$ is the maximum free energy that can contribute to a motor's power stroke (Hill et al. 1975; Fisher and Kolomeisky 1999; Howard 2006; Purcell et al. 2011). This is not a rigorous physical constraint; rather, it is a sensible, first-order approximation that allows us to study evolutionary effects across a wide range of biological machines. We later use a more refined model of F_oF_1-ATPase in order to ask more specific questions about that motor's evolution.

We use this model to study the in vivo operation of 11 of the machines in figure 2, which we split into two classes. Class 1 contains the *driven* machines, classified by the criteria $w^0 \geq 4.5$ kT and $\Delta\mu^0 \geq w^0$. These are myosin II, NCX, NCKX, Animal F_oF_1-ATPases, and *E. coli* F_oF_1-ATPase. The machines in Class II are *ratchet* machines. Here, they are all ion pumps that work primarily against chemiosmotic gradients: Na-K ATPase, SERCA, the proton PP_i pump, PMCA, and V-ATPase (NOTE.—The only machine we do not classify or analyze is chloroplast F_oF_1-ATPase, which has a large value of Δw^0, which would place it in class I, but a very small value of $\Delta\mu^0$.). We calculate the performance landscapes for these two classes of machines in figures 4 and 5.

A Mechanistic Mesoscale Model of F_oF_1-ATPase

We use a discrete, 2D model (for the F_o and F_1 domains) to represent the dynamical steps of F_oF_1-ATPase. The F_o domain rotates as it transports protons downhill, see figure 6. The F_1 domain undergoes cycles of reactant (ADP and P_i) binding, ATP synthesis, and ATP release. The two domains are joined by the elastic linker γ, which has the energy:

$$E_\gamma(\theta_i, \varphi_j) = \frac{1}{2}\kappa(\theta_i - \varphi_j)^2, \tag{12}$$

where κ is a spring constant, θ_i is the angular position of F_o, and φ_j is the preferred angle (that which gives maximal stability) for the jth chemical state of F_1.

Figure 6 illustrates the steps of the F_oF_1 mechanism included in our dynamical model. The F_o domain has three transitions in which F_o binds a proton on the periplasmic (P) side of the membrane, rotates from θ_i to θ_{i+1}, and releases a proton on the cytoplasmic (N) side. The basic free energy changes across each of these three steps are as follows:

$$\begin{aligned} g^{H^+_P}_{on} &= 2.3\left(pK_a^{(P)} - pH^{(P)}\right), \\ g_{rot}(\theta_i, \varphi_j) &= 2.3\left(pK_a^{(N)} - pK_a^{(P)}\right) - F_e\Delta\psi, \\ &\quad + E_\gamma(\theta_{i+1}, \varphi_j) - E_\gamma(\theta_i, \varphi_j) \\ g^{H^+_N}_{off} &= 2.3\left(pH^{(N)} - pK_a^{(N)}\right), \end{aligned} \tag{13}$$

with the apparent pK_a's of the P- and N-sides labeled. The total change in basic free energy across these three steps, found by summing the three equations (13), is equal to $\Delta\mu_{H^+}$, the free energy gained by transporting one proton across the membrane, plus ΔE_γ, the change in elastic energy of the γ-subunit. During ATP synthesis, F_o rotation (the second step) acts as a mechanical step that increases the strain from the elastic linker ΔE_γ. The elastic strain is transmitted to F_1, and then relieved when F_1 undergoes a chemical transition such as ADP binding or ATP release. The basic free energy change of an F_1 transition is as follows:

$$g_{F_1} = \Delta G^{F_1}_{j,j+1} + E_\gamma(\theta_i, \varphi_{j+1}) - E_\gamma(\theta_i, \varphi_j), \tag{14}$$

where j indexes the F_1 state and $\Delta G^{F_1}_{j,j+1}$ is the free energy associated with the component of ATP synthesis from j to $j+1$. Over a full cycle these changes sum to the work of synthesizing three ATP molecules: $\sum_{j=0}^{8} \Delta G^{F_1}_{i,(i+1)\bmod 8} = 3\Delta\mu_{ATP}$.

The model is well constrained by experimental data, including the apparent pK_a's of the c-ring on both sides of the membrane (Gräber 1994; Wiedenmann et al. 2009), the elasticity of the γ-subunit (Wächter et al. 2011), and the angular dependence of rates for the different components of ATP synthesis by the F_1 domain (Watanabe et al. 2011; Adachi et al. 2012; Suzuki et al. 2014). There is a range of final parameter values that affects the absolute synthesis rates but do not affect the qualitative features of figure 7; that is, the synthesis rates in these figures are scaled systematically over a small window. See supplementary section IV, Supplementary Material online, for full details of parameterization and sensitivity analysis.

Supplementary Material

Supplementary data are available at *Molecular Biology and Evolution* online.

Acknowledgments

We thank Sasha Levy and Vageli Coutsias for comments and suggestions. We are grateful for support from the Laufer Center for Physical and Quantitative Biology and from NIH Grant GM06359217.

References

Adachi K, Oiwa K, Yoshida M, Nishizaka T, Kinosita K. 2012. Controlled rotation of the F_1-ATPase reveals differential and continuous binding changes for ATP synthesis. *Nat Commun*. 3(1):1022.

Agozzino L, Dill KA. 2018. Protein evolution speed depends on its stability and abundance and on chaperone concentrations. *Proc Natl Acad Sci U S A*. 115(37):9092–9097.

Ahn W, Lee MG, Kim KH, Muallem S. 2003. Multiple effects of SERCA2b mutations associated with Darier's disease. *J Biol Chem*. 278(23):20795–20801.

Anandakrishnan R, Zhang Z, Donovan-Maiye R, Zuckerman DM. 2016. Biophysical comparison of ATP synthesis mechanisms shows a kinetic advantage for the rotary process. *Proc Natl Acad Sci U S A*. 113:11220–11225.

Astumian RD, Mukherjee S, Warshel A. 2016. The physics and physical chemistry of molecular machines. *ChemPhysChem* 17(12):1719–1741.

Brown AI, Sivak DA. 2017. Allocating dissipation across a molecular machine cycle to maximize flux. *Proc Natl Acad Sci U S A*. 114(42):11057–11062.

Brown AI, Sivak DA. 2018. Allocating and splitting free energy to maximize molecular machine flux. *J Phys Chem B*. 122(4):1387–1393.
Buttgereit F, Brand MD. 1995. A hierarchy of ATP-consuming processes in mammalian cells. *Biochem J*. 312(1):163–167.
Capitanio M, Canepari M, Cacciafesta P, Lombardi V, Cicchi R, Maffei M, Pavone FS, Bottinelli R. 2006. Two independent mechanical events in the interaction cycle of skeletal muscle myosin with actin. *Proc Natl Acad Sci U S A*. 103(1):87–92.
Checchetto V, Segalla A, Allorent G, La Rocca N, Leanza L, Giacometti GM, Uozumi N, Finazzi G, Bergantino E, Szabò I. 2012. Thylakoid potassium channel is required for efficient photosynthesis in cyanobacteria. *Proc Natl Acad Sci U S A*. 109(27):11043–11048.
Clausen MV, Hilbers F, Poulsen H. 2017. The structure and function of the Na, K-ATPase isoforms in health and disease. *Front Physiol*. 8:371.
Dautant A, Meier T, Hahn A, Tribouillard-Tanvier D, Rago JP D, Kucharczyk R. 2018. ATP synthase diseases of mitochondrial genetic origin. *Front Physiol*. 9(329):1–16.
Fisher ME, Kolomeisky AB. 1999. The force exerted by a molecular motor. *Proc Natl Acad Sci U S A*. 96(12):6597–6602.
Gräber P. 1994. The H+-ATPase from chloroplasts: energetics of the catalytic cycle. *Bioenergetics* 1187(2):171–176.
Greenberg MJ, Kazmierczak K, Szczesna-Cordary D, Moore JR. 2010. Cardiomyopathy-linked myosin regulatory light chain mutations disrupt myosin strain-dependent biochemistry. *Proc Natl Acad Sci U S A*. 107(40):17403–17408.
Hill T. 1977. Free energy transduction in biology: the steady-state kinetic and thermodynamic formalism. New York: Academic Press, Inc.
Hill TL, Eisenberg E, Chen YD, Podolsky RJ. 1975. Some self-consistent two-state sliding filament models of muscle contraction. *Biophys J*. 15(4):335–372.
Howard J. 2006. Protein power strokes. *Curr Biol*. 16(14):R517–R519.
Howard J. 2011. Motor proteins as nanomachines: the roles of thermal fluctuations in generating force and motion. In: Rivasseau V, editor. Biological physics. Basel: Springer. p. 47–59.
Howarth C, Gleeson P, Attwell D. 2012. Updated energy budgets for neural computation in the neocortex and cerebellum. *J Cereb Blood Flow Metab*. 32(7):1222–1232.
Kalapis D, Bezerra AR, Farkas Z, Horvath P, Bódi Z, Daraba A, Szamecz B, Gut I, Bayes M, Santos MAS, et al. 2015. Evolution of robustness to protein mistranslation by accelerated protein turnover. *PLoS Biol*. 13(11):e1002291–e1002328.
Klesmith JR, Bacik JP, Wrenbeck EE, Michalczyk R, Whitehead TA. 2017. Trade-offs between enzyme fitness and solubility illuminated by deep mutational scanning. *Proc Natl Acad Sci U S A*. 114(9):2265–2270.
Kucharczyk R, Zick M, Bietenhader M, Rak M, Couplan E, Blondel M, Caubet SD, di Rago JP. 2009. Mitochondrial ATP synthase disorders: molecular mechanisms and the quest for curative therapeutic approaches. *Biochim Biophys Acta*. 1793(1):186–199.
Langenbacher AD, Dong Y, Shu X, Choi J, Nicoll DA, Goldhaber JI, Philipson KD, Chen JN. 2005. Mutation in sodium-calcium exchanger 1 (NCX1) causes cardiac fibrillation in zebrafish. *Proc Natl Acad Sci U S A*. 102(49):17699–17704.
Lee JH, Han J, Kim H, Park SM, Joe E, Jou I. 2019. Parkinson's disease-associated LRRK2-G2019S mutant acts through regulation of SERCA activity to control ER stress in astrocytes. *Acta Neuropathol Commun*. 7(68):1–19.
Lin T, Greenberg MJ, Moore JR, Ostap EM. 2011. A hearing loss-associated myo1c mutation (R156W) decreases the myosin duty ratio and force sensitivity. *Biochemistry* 50(11):1831–1838.
Oster G, Wang H. 2000. Reverse engineering a protein: the mechanochemistry of ATP synthase. *Biochim Biophys Acta*. 1458(2–3):482–510.
Paul J. 1965. Carbohydrate and energy metabolism. In: Willmer E, editor. Cells and tissues in culture. New York: Academic Press. p. 239–276.
Piazzesi G, Reconditi M, Linari M, Lucii L, Bianco P, Brunello E, Decostre V, Stewart A, Gore DB, Irving TC, et al. 2007. Skeletal muscle performance determined by modulation of number of myosin motors rather than motor force or stroke size. *Cell* 131(4):784–795.
Pogoryelov D, Klyszejko AL, Krasnoselska GO, Heller EM, Leone V, Langer JD, Vonck J, Muller DJ, Faraldo-Gómez JD, Meier T. 2012. Engineering rotor ring stoichiometries in the ATP synthase. *Proc Natl Acad Sci U S A*. 109(25):E1599–E1608.
Pogoryelov D, Yildiz Ö, Faraldo-Gómez JD, Meier T. 2009. High-resolution structure of the rotor ring of a proton-dependent ATP synthase. *Nat Struct Mol Biol*. 16(10):1068–1073.
Preiss L, Klyszejko AL, Hicks DB, Liu J, Fackelmayer OJ, Yildiz O, Krulwich TA, Meier T. 2013. The c-ring stoichiometry of ATP synthase is adapted to cell physiological requirements of alkaliphilic *Bacillus pseudofirmus* OF4. *Proc Natl Acad Sci U S A*. 110(19):7874–7879.
Purcell TJ, Naber N, Franks-Skiba K, Dunn AR, Eldred CC, Berger CL, Málnási-Csizmadia A, Spudich JA, Swank DM, Pate E, et al. 2011. Nucleotide pocket thermodynamics measured by EPR reveal how energy partitioning relates myosin speed to efficiency. *J Mol Biol*. 407(1):79–91.
Sabater-Muñoz B, Prats-Escriche M, Montagud-Martínez R, López-Cerdán A, Toft C, Aguilar-Rodríguez J, Wagner A, Fares MA. 2015. Fitness trade-offs determine the role of the molecular chaperonin GroEL in buffering mutations. *Mol Biol Evol*. 32(10):2681–2693.
Sakamoto T, Yildez A, Selvin PR, Sellers JR. 2005. Step-size Is determined by neck length in myosin V. *Biochemistry* 44(49):16203–16210.
Santra M, Farrell DW, Dill KA. 2017. Bacterial proteostasis balances energy and chaperone utilization efficiently. *Proc Natl Acad Sci U S A*. 114(13):E2654–E2661.
Schmiedl T, Seifert U. 2008. Efficiency of molecular motors at maximum power. *Europhys Lett*. 83(3):30005.
Sherwood JJ, Waller GS, Warshaw DM, Lowey S, Spudich JA. 2004. A point mutation in the regulatory light chain reduces the step size of skeletal muscle myosin. *Proc Natl Acad Sci U S A*. 101(30):10973–10978.
Shoval O, Sheftel H, Shinar G, Hart Y, Ramote O, Mayo A, Dekel E, Kavanagh K, Alon U. 2012. Evolutionary trade-offs, Pareto optimality, and the geometry of phenotype space. *Science* 336(6085):1157–1160.
Sikosek T, Chan HS. 2014. Biophysics of protein evolution and evolutionary protein biophysics. *J R Soc Interface*. 11(100):20140419.
Sikosek T, Chan HS, Bornberg-Bauer E. 2012. Escape from adaptive conflict follows from weak functional trade-offs and mutational robustness. *Proc Natl Acad Sci U S A*. 109(37):14888–14893.
Spiller S, Friedrich T. 2014. Functional analysis of human Na^+/K^+-ATPase familial or sporadic hemiplegic migraine mutations expressed in *Xenopus* oocytes. *World J Biol Chem*. 5(2):240–253.
Suzuki T, Tanaka K, Wakabayashi C, Saita E, Yoshida M. 2014. Chemomechanical coupling of human mitochondrial F_1-ATPase motor. *Nat Chem Biol*. 10:930–936.
Tokuriki N, Stricher F, Serrano L, Tawfik DS. 2008. How protein stability and new functions trade off. *PLoS Comput Biol*. 4(2):e1000002.
Toyoshima C. 2009. How Ca2+-ATPase pumps ions across the sarcoplasmic reticulum membrane. *Biochim Biophys Acta*. 1793(6):941–946.
Van den Broeck C. 2005. Thermodynamic efficiency at maximum power. *Phys Rev Lett*. 95(19):190602.
von Ballmoos C, Wiedenmann A, Dimroth P. 2009. Essentials for ATP synthesis by F_1F_o ATP synthases. *Annu Rev Biochem*. 78(1):649–672.
Wächter A, Bi Y, Dunn SD, Cain BD, Sielaff H, Wintermann F, Engelbrecht S, Junge W, Walker JE. 2011. Two rotary motors in F-ATP synthase are elastically coupled by a flexible rotor and a stiff stator stalk. *Proc Natl Acad Sci U S A*. 108(10):3924–3929.
Wagoner JA, Dill KA. 2016. Molecular motors: power strokes outperform Brownian ratchets. *J Phys Chem B*. 120(26):6327–6336.
Wagoner JA, Dill KA. 2019. Mechanisms for achieving high speed and efficiency in molecular machines. *Proc Natl Acad Sci U S A*. 116(13):5902–5907.

Watanabe R, Okuno D, Sakakihara S, Shimabukuro K, Iino R, Yoshida M, Noji H. 2011. Mechanical modulation of catalytic power on F_1-ATPase. *Nat Chem Biol*. 8(1):86–92.

Watt IN, Montgomery MG, Runswick MJ, Leslie AGW, Walker JE. 2010. Bioenergetic cost of making an adenosine triphosphate molecule in animal mitochondria. *Proc Natl Acad Sci U S A*. 107(39):16823–16827.

Wiedenmann A, Dimroth P, von Ballmoos C. 2009. Functional asymmetry of the F_o motor in bacterial ATP synthases. *Mol Microbiol*. 72(2):479–490.